Assembling Carbon Nanotube Architectures

Michael Dasbach, Markus Pyschik, Viktor Lehmann, Kristian Parey, Daniel Rhinow, Hendrik M. Reinhardt, and Norbert A. Hampp*

Read Online

ACCESS | Metrics & More | Article Recommendations | Supporting Information

ABSTRACT: Well-defined multiwalled carbon nanotube structures are generated on stainless steel AISI 304 (EN AW 1.4301) by chemical vapor deposition. Pulsed laser-induced dewetting (PLiD) of the surface, by 532 nm nanosecond laser pulses, is utilized for the preparation of metal oxide nanoparticle fields with a defined particle number per area. The reduction of the precursor particles is achieved in an Ar/H_2 (10% H_2) atmosphere at 750 °C, thereby generating catalytic nanoparticles (c-NPs) for carbon nanotube (CNT) growth. Ethylene is used as a precursor gas for CNT growth. CNT lengths and morphology are directly related to the c-NP aerial density, which is dependent on the number of dewetting cycles during the PLiD process. Within a narrow window of c-NP per area, vertically aligned carbon nanotubes of great lengths are obtained. For more intense laser treatments, three-dimensional dewetting occurs and results in the formation of cauliflower-like structures. The laser process enables the creation of all kinds of CNT morphologies nearby on the microscale.

KEYWORDS: *carbon nanotubes, pulsed laser-induced dewetting, catalytic nanoparticles, vertically aligned CNTs, cauliflower structures*

In recent years, much research has focused on nanotechnology and nanocomposites. Carbon nanotubes (CNTs), due to their multifunctional properties, are promising candidates in these fields of applications. Their high compression strength,[1] ballistic conduction,[2] and super-hydrophobicity,[3] as well as their light weight and high aspect ratio, make them favorable additives for composite materials such as polymers,[4] ceramics,[5] and metals[6] with applications as sensors,[7] transistors,[8] energy and data storage devices,[9,10] solar cells,[11] and human health devices.[12] Most commonly, chemical vapor deposition (CVD) is used for the generation of CNTs since the amount of generated CNTs is superior compared to arc discharge or laser ablation techniques.[13] For both quality and quantity of CNTs generated by CVD, the catalyst performance is a crucial factor. Typically, nanoparticles of transition metals such as iron, cobalt, or nickel are used. However, other metals, such as chromium, have been found, which although not functioning as catalysts themselves, can improve the catalytic properties of the sample.[14] The size and form of the particles define the resulting diameter of the generated nanotubes. During the CVD process, the hydrocarbon gas gets cracked into hydrogen and carbon at the surface region of the particles, whereby carbon dissolves in the catalyst, generating a carbon-supersaturated state, which afterward results in tubelike precipitation of carbon on the surface.[15] Under continuous carbon feed, the structure rises, with the catalyst nanoparticle embedded at the tip (tip growth)

or the base (base growth) of the evolving CNT.[16] The adsorption between particle and substrate controls the growth mechanism.[17] Recently, stainless steel gained significant attention due to its great accessibility and the advantage of providing catalysts for CNT growth, as well as being a conductive substrate. Direct growth of CNTs on stainless steel offers the possibility of transferring CNT functionalities directly onto the metal, delivering a better connection between substrate and CNTs. It was found that the mechanical performance of CNTs is dependent on the surface morphology as well as the exact material composition of stainless steel.[18] The good processability of stainless steel enables a wide range of substrate structures, such as meshes,[19] tubes,[20] powders,[21] or thin foils,[22] making it promising for multiple applications. Therefore, there are plenty of strategies for generating CNTs directly on stainless steel, such as radio frequency-powered plasma-enhanced chemical vapor deposition (PECVD),[23] microwave plasma chemical vapor deposition (MPCVD),[24] or flame synthesis.[25] However, those techniques typically lack good alignment or require intensive pretreatments. Preceding
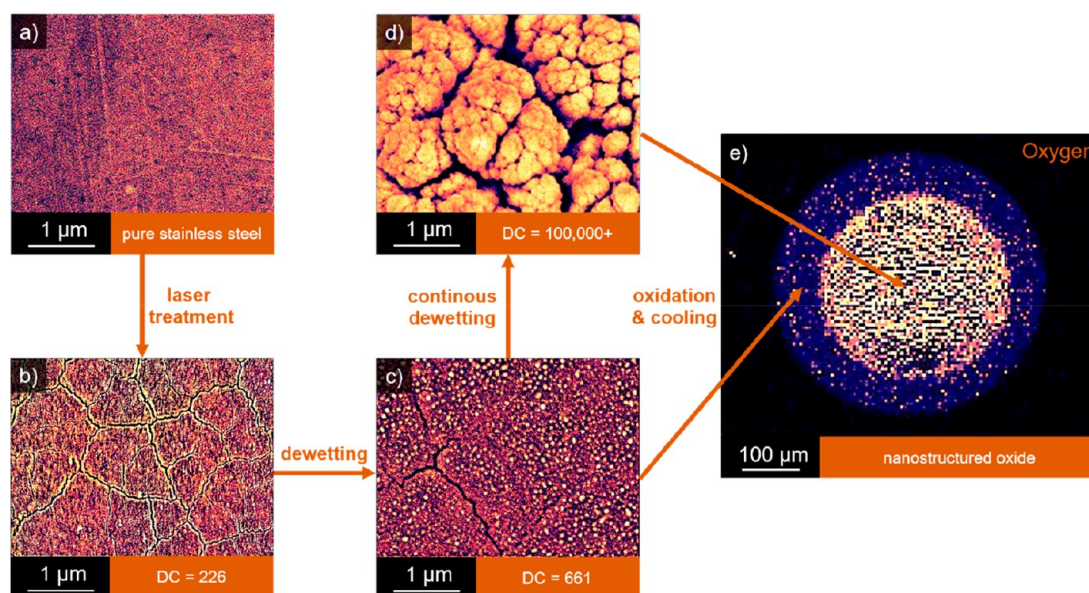
Figure 1. Preparation of stainless steel substrates for CNT growth by pulsed laser-induced dewetting (PLiD). Stainless steel surface (a) before and (b−d) after defined numbers of PLiD steps (secondary electron, SE, detector). The number of metal oxide NPs on the surface is related to the number of DCs applied. (e) Oxygen analysis (energy dispersive X-ray, EDX, detector) of an area where a high density (middle) and a low density (surrounding ring) of oxidized nanoparticles have been prepared. The repetition of the process changes the morphology of the particles, enabling the adjustment of their catalytic properties. During the following CVD process, the surface gets reduced, forming metallic c-NPs, which enable the CNT growth. $\varphi = 0.34$ J cm^{-2}.
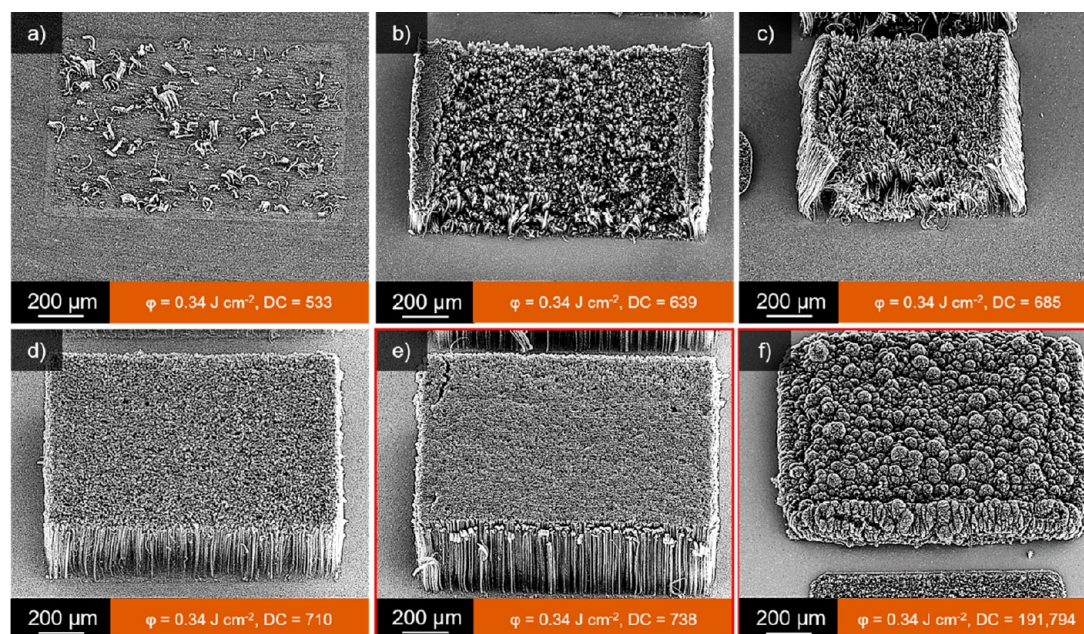
Figure 2. CNT growth on differing catalyst densities per area. (a−f) Catalyst precursors were synthesized with an increasing number of DCs with all other parameters left constant: (a) DC = 533, (b) DC = 639, (c) DC = 685, (d) DC = 710, (e) DC = 738, (f) DC = 191,794, $\varphi = 0.34$ J cm^{-2}. Picture angle 40°. (e, f) (red framed) Two selected preparation conditions used for all further discussions.

oxidation of the stainless steel surface increases the yield of CNTs obtained during the CVD process because oxidation leads to an increase of the surface area as well as an increase in the density of crystallographic defects.[19] Both propagate the treated regions for CNT growth as soon as the reduction to metallic nanoparticles during CVD treatment occurs.[26,27] Besides the nanoparticles, surface crevices also appear to be a crucial parameter for a number of catalytic sites.[28] A promising method for catalyst particle generation is the use of

pulsed lasers, stimulating the surface for CNT growth.[29,30] In recent studies, we showed that by pulsed laser-induced dewetting (PLiD) of a stainless steel surface the catalytic properties of laser-generated nanoparticles may be optimized very precisely.[31] Dewetting cycles (DCs) of PLiD are known to provide rapid thermal heating and cooling rates of up to 10^{10} K s^{-1}.[32] Rapid temperature dissipation from the surface region into the bulk causes supercooling of the surface, thus leading to the quenching of metastable intermediate states.[33−35] In this
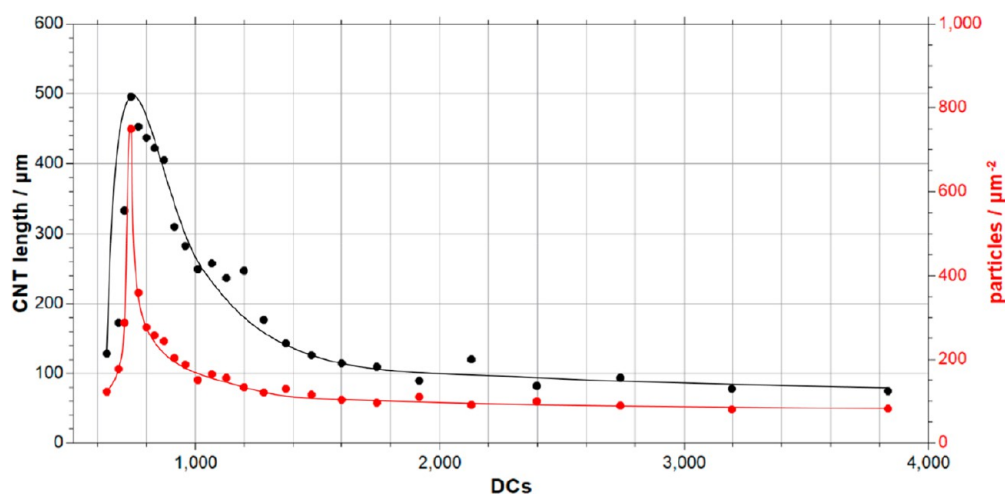
Figure 3. CNT lengths (left axis) obtained as a function of particle density (right axis) compared to the underlying number of DCs. $\varphi = 0.34$ J cm^{-2} (see also Figure S1).

study, we take a closer look at the growth behavior of CNTs in reliance on the underlying catalyst density per area, which is dependent on the laser treatment of the sample. We demonstrate optimized parameters for obtaining vertically aligned CNTs (VA-CNTs) on surface-dewetted stainless steel substrates and compare them to CNTs obtained from three-dimensional dewetted cauliflower-like surface structures (CF-CNTs). The degree of dewetting is controlled by the number of laser pulses interacting with the sample surface. Each pulse triggers a DC, promoting the generation of spherical nanoparticles and initiating crevices and three-dimensional dewetting culminating in cauliflower structures. Controlling the surface structure of stainless steel facilitates controlling the CNT growth behavior itself by adjusting the amount of c-NPs per area.

RESULTS AND DISCUSSION

During laser processing the stainless steel surface melts, provoking an unstable surface state which relaxes by forming crevices and dewetting of the liquefied metal film into oxidized nanoparticles. Repetition of this process leads to changes in the morphology of the particles and the underlying surface, enabling the adjustment of catalytic properties of the sample itself, without the necessity to add additional catalytic material. During the CVD process, the oxidized precursors are reduced to metallic particles, forming the catalysts for CNT growth. The whole synthesis process is depicted in Figure 1.

Figure 1 shows the generation process of oxidized nanoparticles during PLiD. Each particle generation process is triggered by a new dewetting pass, *i.e.*, by an additional laser pulse interacting with the sample. The number of DCs precisely controls the amount, as well as the geometry, of the resulting particles, in turn generating the catalysts for CNT growth. Generally, the use of stainless steel as a catalyst for CNT growth is somehow complicated. When untreated, the stainless steel surface is layered by a protective chromium oxide layer, prohibiting carbon absorption during the CVD process.[19,36] Typically the eradication of the protective layer and further on the generation of the catalytic particles of stainless steel are obtained *via* plasma treatment[23] or surface etching, whereby particular catalysts are formed by increasing the surface roughness of the sample by acids, such as hydrochloric acid[37] or sulfuric acid.[38] The superiority of

PLiD lies in the fact that no chemical pretreatment of the sample is required, making it less time-consuming, as well as easier and more precise to adjust.

For the generation of VA-CNTs, we found 738 DC at a pulse fluence of $\varphi = 0.34$ J cm^{-2} to be optimal. These conditions correspond to a c-NP density of about 750 nanoparticles/μm^2. In Figure 2e, a field of VA-CNT, grown with the parameters mentioned above, is shown. The density of CNTs is optimal for a self-stabilizing effect, leading to a well-aligned structure with a CNT length of 500 μm. Figure 2 shows the relation between the DCs applied to the sample and the resulting CNT growth behavior. From (a) to (f) the number of DCs increases, with a drastic final raise from (e) to (f). All CNTs were obtained under identical CVD conditions. Figure 2a shows a sample with 533 DCs where only a few nanotubes are found after CNT growth. The catalyst density of the sample is quite low, not even resulting in a fully covered surface. When the amount of DCs is adjusted the number of grown CNTs increases, too. Six hundred thirty-nine DCs already lead to a fully overgrown surface (Figure 2b), but the CNTs are not aligned. Starting from 685 DCs the surface conditions lead to a somehow erected CNT growth, indicating the vertical alignment of the nanostructures. In Figure 2d,e, fully VA-CNTs are obtained, however, still differing in size and density. The less dense catalyst field obtained from 710 DCs Figure 2d, in comparison to the one obtained from 738 DCs, Figure 2e, leads to less dense CNT growth. In addition, the lower particle amount in Figure 2d leads to an earlier carbon saturation of the catalysts during CVD, resulting in a shorter length of the CNTs. When the amount of DCs is drastically increased, the growth behavior of the CNTs also changes (Figure 2f). Instead of growing vertically, the CNTs tend to rise chaotically, generating a bulged structure lacking any alignment.

The change in the CNT growth behavior is caused by a change in the surface structure of stainless steel. Each DC not only triggers the formation of nanoparticles but also leads to the formation of crevices, destroying the top layer of the surface and leading to a significant increase of the surface roughness. This quasi three-dimensional dewetting process generates so-called cauliflower structures and completely disintegrates the surface of the sample. The obtained structure consists of multiple nanostructured microstructures, without
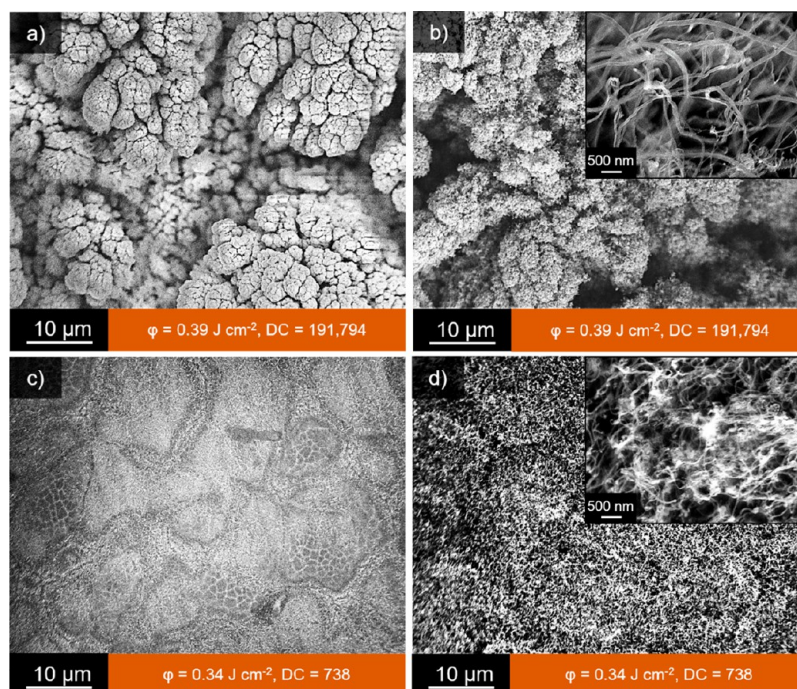
Figure 4. Comparison of three-dimensional dewetted, so-called cauliflower-like field (a and b), and two-dimensional dewetted catalyst field (c and d), before (a and c) and after (b and d) CNT growth. a) $\varphi = 0.39$ J cm^{-2}, DC = 191,794 c) $\varphi = 0.34$ J cm^{-2}, DC = 738. (Insets in b and d show magnified images of the CNT fields.)
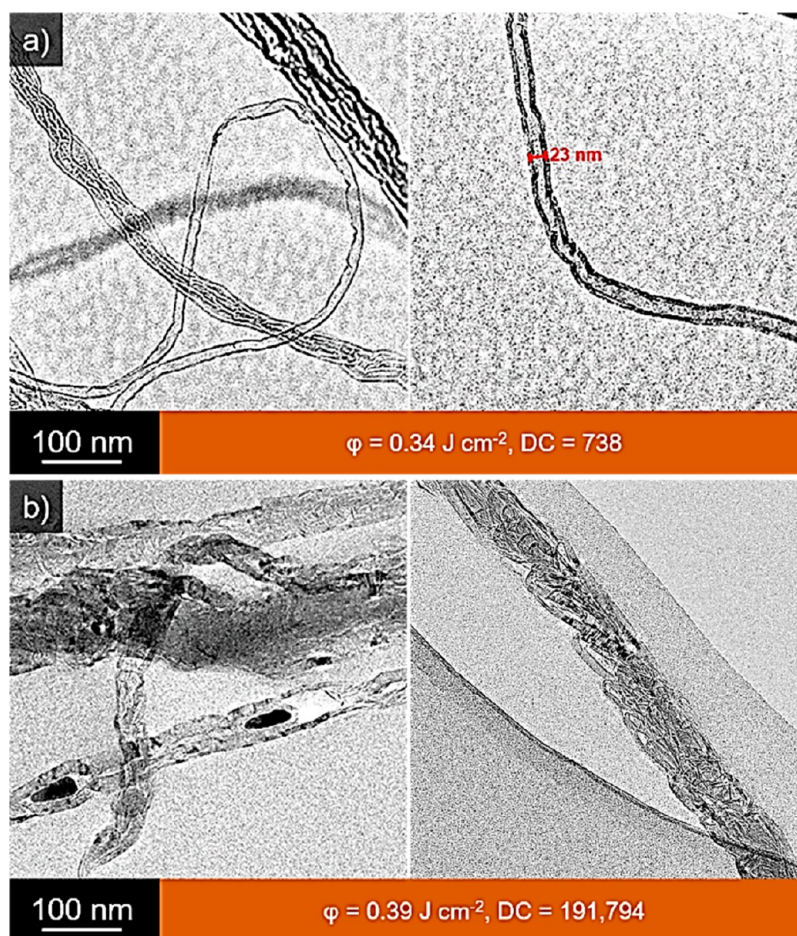
Figure 5. TEM images of (a) VA-CNTs and (b) CF-CNTs. (a) Width of the VA-CNTs match the c-NP size. $\varphi = 0.34$ J cm^{-2}, DC = 738. (b) CF-CNTs contain multiple c-NPs. $\varphi = 0.39$ J cm^{-2}, DC = 191,794.
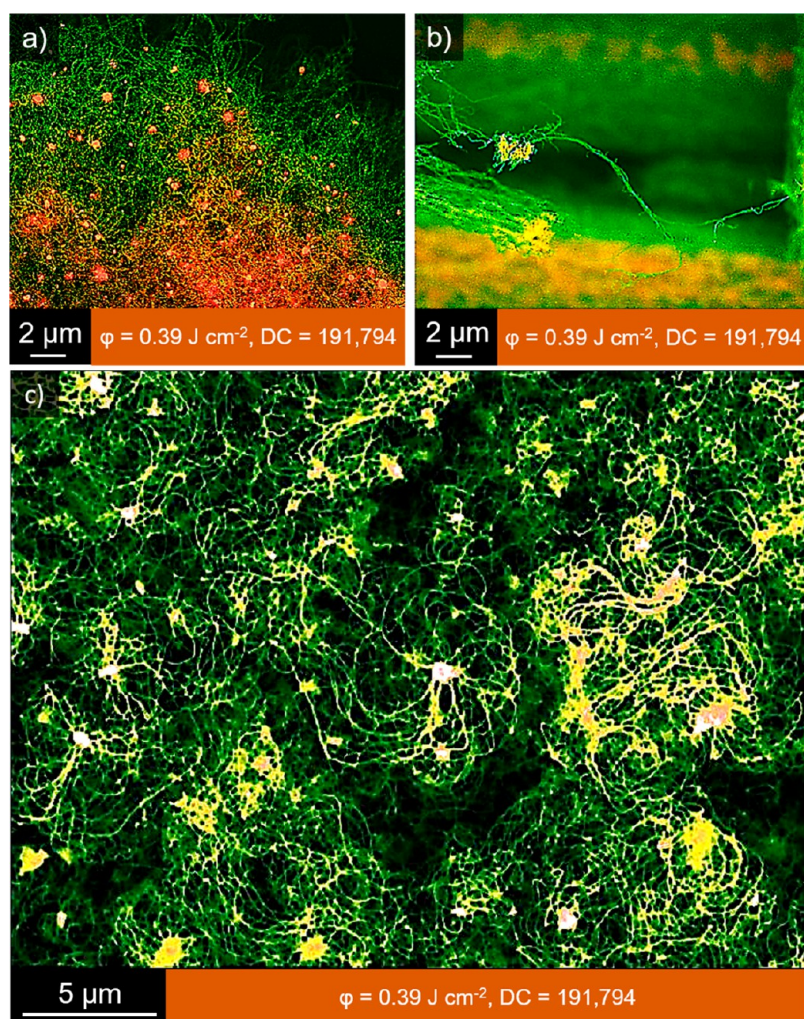
Figure 6. CF-CNTs with entrapped metal clusters. Carbon structures are pictured in green, whereby metallic catalysts are illustrated red/yellow. (a, b) Overlay of secondary and backscattered electron detectors. (c) Secondary electron image. $\varphi = 0.39$ J cm^{-2}, DC = 191,794.

any kind of order, however, still containing dewetted particles. When comparing the catalytic growth conditions VA-CNTs can be produced over a broad number of underlying DCs. When rising the number of DCs, once good stabilization is reached, CNTs always tend to grow vertically aligned until CF structures occur. Following a comparison of the obtained length, as well as particle density per μm^2 and the underlying DCs are given in Figure 3. It strikes that ideal growth conditions can only be reached by a well-defined number of DCs. However, CNTs with a length of roughly 100 μm can be generated over a large range of underlying DCs. Once surpassing 4000 DCs cauliflower-type development is introduced, making it impossible to determine the exact CNT length.

When comparing obtained CNT lengths and the underlying c-NP density, both can be found culminating in a rather narrow window around 738 DCs. Even a small deviation from the optimal c-NP density leads to a massive decrease in CNT length, picturing the sensitivity and relevance of the catalytic system.

In Figure 4, a cauliflower-like surface structure, (a) and (b), is compared with a VA-CNT sample, (c) and (d), before, (a) and (c), and after CNT generation, (b) and (d). When comparing the raw catalyst fields, the enormous change in the surface structure, due to three-dimensional dewetting, is seen.

Cauliflower structures consist of inhomogeneous bulky outgrowths, whereas the two-dimensional dewetted sample is almost planar. Analogous to the catalyst layer structure, also the order of the obtained CNTs differs. Due to the three-dimensional catalyst distribution CF-CNTs tend to grow chaotically, lacking any form of alignment. Two-dimensional catalyst arrays in contrast lead to homogeneous CNT films, self-stabilizing as VA-CNTs.

When taking a closer look at the appearance of the carbon structures arising from a cauliflower surface, a combination of carbon nanofibers (CNFs) and CNTs is found. Diameters of filamentous carbon structures, arising during CVD, strongly depend on the diameter of the underlying catalysts. Catalytic structures with a diameter below 60 nm trigger multiwalled CNTs (MWCNTs), whereas structures with a diameter above 60 nm strongly favor the generation CNFs.[39] For both dewetting conditions, VA-CNTs, and CF-CNTs, catalyst diameters below 60 nm can be found (VA-CNTs: 26.3 nm ± 2.4 nm; CF-CNTs: 16.2 nm ± 1.7 nm) enabling the growth of MWCNTs. However, as indicated in Figure 4a), the massive surface treatment, in the case of CF-CNT catalysts, leads to the development of bulky structures above 60 nm in diameter. The different diameters of the carbon structures resulting from the combination of nanoparticles and the bulky primary structure, lead to the development of CNTs as well as CNFs. For
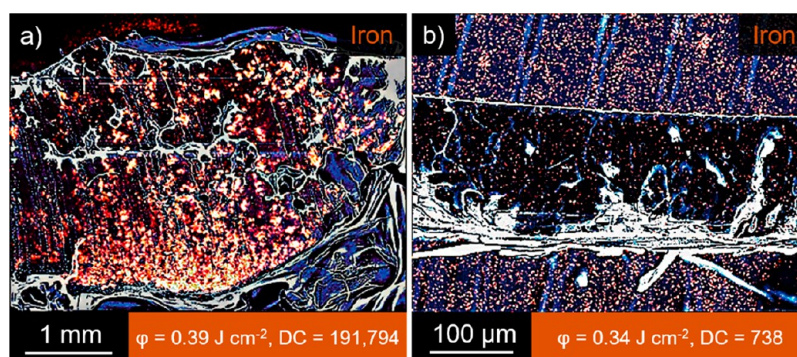
Figure 7. Cross sections of CF-CNT (a) and VA-CNT (b) silicone films. The CNTs on top of the steel substrates were soaked with silicone, polymerized, and removed from the substrates. SE images (bluish) are superimposed with the corresponding iron EDX mappings (orange). a) In the CF-CNT films, the iron nanoparticles (red) are found throughout the whole film. b) A different picture is seen in the VA-CNT films, where almost any iron nanoparticles are inside the film. (a) $\varphi = 0.39$ J cm^{-2}, DC = 191,794; (b) $\varphi = 0.34$ J cm^{-2}, DC = 738.
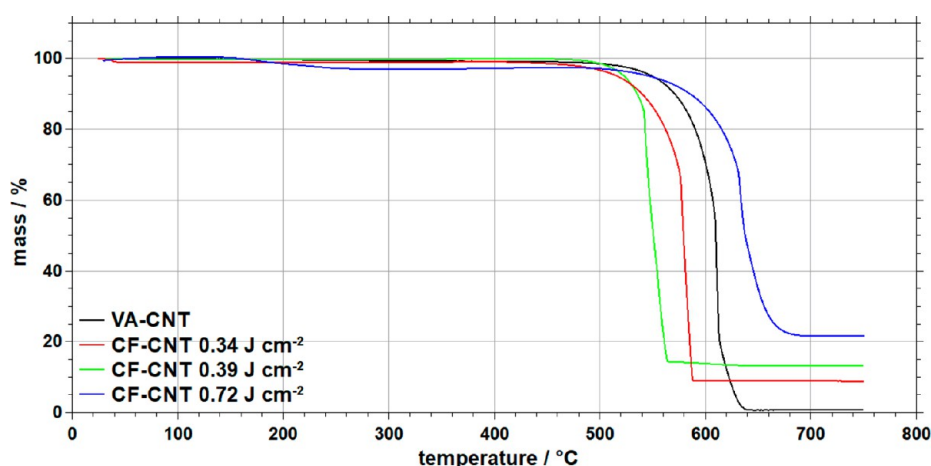
Figure 8. Thermogravimetric analysis (TGA) of VA-CNTs and CF-CNTs. VA-CNT catalysts: $\varphi = 0.34$ J cm^{-2}, DC = 738. CF-CNT catalysts: $\varphi = 0.34$ J cm^{-2}, 0.39 J cm^{-2} and 0.72 J cm^{-2}, DC = 191,794. The higher the fluence applied, the higher the contained metal content is. (see also Figure S2).

consistency reasons, structures arising from cauliflower catalysts will further on still be mentioned as CF-CNTs. In Figure 5 TEM images of VA-CNTs (a) and CF-CNTs (b) are shown.

For both VA-CNTs and CF-CNTs, nanotubes can be identified, consisting of a well-defined cylindrical wall layer. VA-CNTs exhibit a diameter of 23 nm, identical to the underlying catalyst particle size. However, in the case of CF-CNTs embedded particles can also be found, increasing the total diameter of the CNTs. Additionally, CNFs consisting of stacked cones of graphene can be obtained.

Besides the c-NP density and size on the surface, also the catalyst adhesion to the substrate surface affects the CNT growth. Due to the disintegration of the top layer of the substrate, the c-NPs are less likely to remain on the surface during the CNT growth proceeds. Parts a and b of Figure 6 show a SE and backscattered electron (BSE) overlay of CF-CNTs. A large amount of remaining c-NP (red/yellow) in the CNT matrix indicates the relatively low adhesion between the substrate and the c-NPs. However, the catalysts are not only embedded in the nanotubes but rather remain in a clustered arrangement. The whole particle clusters get released from the surface during the growth process and are entwined by CNTs. In Figure 6b, a catalyst cluster of roughly 2 μm diameter carried by a CNT strain is presented. The lifted c-NP remains

active during the CNT growth process, providing a base for new carbon adhesion. Figure 6c shows catalyst clusters functioning as seeds for multiple nanotubes at once. However, this leads to a loss of order, since the CNTs grow in any direction.

For the comparison of the amount of c-NPs, the CNT samples were soaked with silicon. Subsequently, cross sections of the obtained films were prepared and analyzed via EDX mapping. In previous studies of our group, iron was found to be the main catalyst relevant for CNT generation from a laser-treated stainless steel sample.[31] In addition, near edge local atomic investigation studies by energy loss spectroscopy (EELS) showed that during CNT growth on stainless steel, small particles get embedded into the nanotube, consisting of no other alloy material but iron.[40] Figure 7 shows an overlay of SE images (blue) and an iron EDX mapping (orange) of cross sections soaked with silicon. Figure 7a shows the cross-section of CF-CNTs, whereas in Figure 7b the VA-CNT cross-section is pictured. CF-CNTs contain plenty of catalyst particles, mainly located at the top and the bottom of the film, but also distributed throughout the whole film. Depending on the surface morphology, stainless steel shows both base and tip growth mechanism. Base growth conditions can be found when the surface gets reconstructed into "nanohills", but remain more or less plane. However, a tip growth mechanism

can be found when surface breakups exist, typically leading to an increase in CNT diameter.[39] The relatively broad distribution of "base and tip growth zone" is due to the low order in the growth direction. This chaotic spreading, as well as the fact of lifting whole particle clusters, contributes to a less defined base and tip zone. In contrast, EDX analysis of VA-CNTs shows practically no iron remaining inside the CNT film.

When comparing both sample types *via* thermogravimetric analysis, the portion of remaining metal particles is analyzed quantitatively. Figure 8 shows TGA data of different CF-CNTs samples and VA-CNTs. The amount of catalysts remaining in the sample correlates to the applied laser fluence. An increase of the energy leads to a stronger disintegration of the surface and, thus, to a higher amount of catalyst clusters only weakly attached to the surface and easy to be lifted off. In parallel, a massive increase in the yield of CNTs is observed. For CF-CNTs metallic amounts of 21.5%, 13.2%, and 8.8% were found, dependent on the laser pulse fluence (0.72, 0.39, 0.34 J cm^{-2}). In contrast, TGA analyses of VA-CNTs show only a metallic amount of 0.7%, 10- to 30-fold less than with CF-CNTs. The high amount of catalysts in the CF-CNTs has two effects. First, the yield of the generated CNTs drastically increases, since any catalyst acts as a seed for multiple nanotubes. Due to the catalyst lifted off a somehow lamellar catalyst system is obtained, leading to a multiorigin CNT network of great length. Due to the primary cauliflower-like surface of the sample, vertical stacking of catalysts cannot be achieved. Compared to typical lamellar catalyst stacking methods, such as by a fluidized bed catalyst, the obtained CNTs show very low order[41] but provide a great yield, are easy to adjust by varying the pulse fluence of the laser. Second, iron, as a ferromagnetic material, leads to a magnetizable CNT structure. The left image in Figure 9 shows a CF-CNT bundle of about 20 mm length. To the right, a part of a CF-CNT bundle is lifted by a small samarium–cobalt magnet.
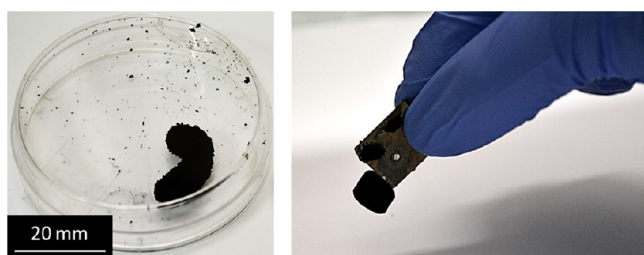
Figure 9. Photography of a CF-CNT bundle. The left image shows a CNT bundle, grown on a cauliflower catalyst field (φ = 0.72 J cm^{-2}, DC = 191,794). The size of the bundle is about 20 mm. On the right side, a piece of such a CNT bundle is attracted by a samarium–cobalt magnet.

The obtained catalyst geometry on stainless steel can be adjusted very precisely by PLiD, allowing the design of any form of catalytic systems on a sample. In Figure 10 a treelike CNT structure is obtained by combining a cauliflower catalyst field in the central region, surrounded by VA-CNTs. VA-CNTs hereby function as shaping cage, defining the orientation of the CF-CNT and thus limiting the degree of chaotic growth behavior. Once the size of the CF-CNTs surpasses the VA-CNT size, the limitation in growth direction vanishes, resulting again in multidirectional propagation.
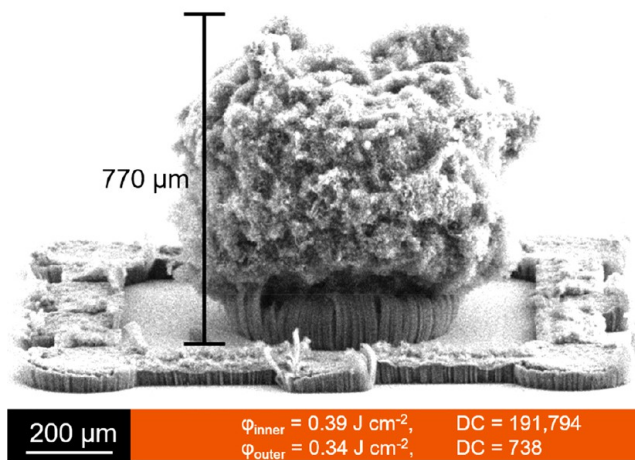
Figure 10. Combination of two-dimensional dewetted (VA-CNT) and three-dimensional dewetted, cauliflower-like catalyst systems. CF-CNTs were produced in an inner circular region surrounded by a two-dimensional dewetted catalyst field. During the growth process, the VA-CNTs in the outer sphere stabilize the growth of the chaotically growing CF-CNTs in the center. CF-CNT area: φ = 0.39 J cm^{-2}, DC = 191, 794, VA-CNT area: φ = 0.34 J cm^{-2}, DC = 738. Picture angle 80°. (Details of the growth kinetics are found in Figure S3).

The control of the growth behavior, size, density, and orientation of CNTs enables the design of microarchitectures. De Volder *et al.* achieved microstructures of CNTs by combining multiple catalyst systems, as well as adjustment of the size and form of the underlying catalyst particles by using lithographic masks.[42] For postprocessing structuring of CNTs water can be used. Qu *et al.* showed that the capillarity effect of CNTs can be exploited to reconstruct the appearance of CNT forests.[43] However, the process of PLiD can be performed maskless and no additional postgrowth treatment is needed. A demonstration of the potential is given in Figure 11 in a more complex structure.

In general, the possibility of locally growing CNTs is highly promising for applications like transistors, field emitters, or sensors. Therefore, plenty of research has been undertaken to obtain locally controlled CNT growth, such as removing parts
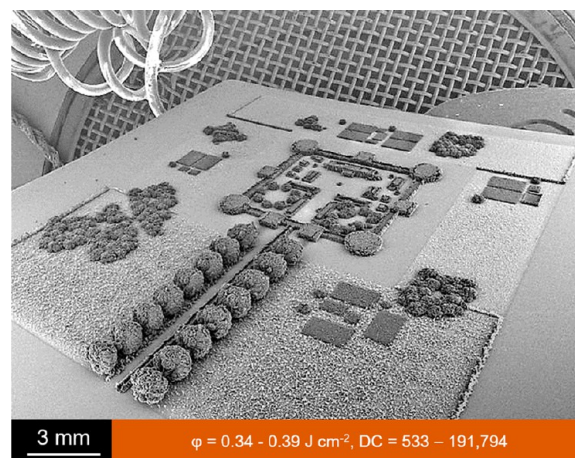
Figure 11. Microarchitecture of a CNT-castle surrounded by a CNT-park. Picture angle 40°.

of the catalyst layer by lithographic methods.[44−47] However, even if enabling the local growth, these methods typically lack the possibility of size control of the obtained CNTs. Therefore, local heat controlled techniques by microresistive heaters[48] or laser-assisted CVD (LACVD)[49] got developed, though being complicated in implementation. Generating catalysts by PLiD enables locally differing growth of CNTs with sharp edges, by just controlling the used laser parameters, providing an easy, fast, and highly controllable catalyst generation method.

CONCLUSIONS

We have presented different growth behaviors of CNTs, depending on the catalyst density per area on the surface, which may be precisely tuned by the number of PLiD cycles applied to produce the catalytic nanoparticles. All experiments were done on simple stainless steel, AISI 304 (EN AW 1.4301). Increasing the numbers of DCs leads to an increase in catalyst precursor particles. Dependent on the particle density, CNT growth occurs more or less aligned. At the experimental conditions employed an optimum for VA-CNT growth was found at 738 DCs at a laser pulse fluence of $\varphi = 0.34$ J cm^{-2}. When drastically increasing the amount of DCs, the surface of the sample completely disintegrates, producing huge amounts of catalytic nanoparticles on a rough cauliflower-like substrate surface. CVD then creates a chaotic CNT growth. Catalysts are entrapped by the growing CNTs and distributed throughout the forming CNT network. A high amount of metallic particles in the obtained CNT network supports this model. Each particle lifted by the nanotubes serves as a seed for additional CNTs, leading to a distributed catalyst system, increasing the total height of the structure. The number of metallic particles is directly related to the used total laser pulse fluence. The advantage of laser-generated catalyst fields for CNT generation lies in its high reproducibility. Catalytic parameters can be adjusted over a broad area, providing multiple levels of CNT growth behavior. The size and form of particle fields can be well-defined, thus enabling placements of multiple catalyst fields with sharp edges beside each other, making this an ideal additive manufacturing technique on the microscale. Due to the different behavior of VA-CNTs and CF-CNTs, the possibility of device production with locally differing properties is given, e.g., alternating regions of isotropic (CF-CNT) and anisotropic (VA-CNT) conductivity or devices with locally differing mechanical stiffness just by varying the degree of chaotic entanglement of the CNTs. Laser processing is a very fast method for the in situ generations of catalytic precursor particles, as well as a yield increasing oxide layer. This facilitates the possibility of an assembly line technology, whereby catalysts get generated directly on a moving thin film, followed by CVD procedure and connected harvesting.

MATERIALS AND METHODS

Yacht polished rolled stainless steel AISI 304 (EN AW 1.4301) was used as a substrate for catalyst generation. A frequency-doubled nanosecond pulsed Nd:YVO$_4$-laser, emitting laser pulses of 5 ns pulse width at a wavelength of 532 nm (Explorer XP 532-5, Newport, USA), was used for catalyst precursor formation. The laser beam was scanned over stainless steel with a line spacing of 3 μm, a pulse repetition rate of $f = 50$ kHz, and various scan speeds over a range of $v = 0.7$ mm s^{-1} up to $v = 240$ mm s^{-1}, controlling pulse overlaps of the laser and thus the number of DC applied to the sample, DC = 191,794 down to DC = 533. A galvanometer scan head (SCANgine 14-532, Scanlab, Germany), equipped with an F-Theta lens (Rodenstock, $f = 163$ mm, Germany), focuses the laser beam to a

spot diameter of 100 μm (1/e2). Two-dimensional dewetted particle fields were made by using a laser fluence per pulse of $\varphi = 0.34$ J cm^{-2}. For the generation of cauliflower-like surface structures a laser fluence per pulse of $\varphi = 0.34$, 0.39, or 0.72 J cm^{-2} was used. For CNT growth the samples were placed in a horizontal quartz glass furnace (35 mm inner diameter, 150 mm heating zone) at 750 °C with a heating rate of 16 °C min^{-1}. Hydrostar 10 (Ar/H$_2$ 90/10; 100 L h^{-1}) was used as the carrier gas, and ethylene gas (6 L h^{-1}) was added for 10 min as the precursor for CNT growth. Samples were placed at a downstream furnace position to achieve optimal growth conditions. For EDX analysis cross sections of silicone soaked CNT films were prepared. CNTs and catalyst fields were analyzed on field emission scanning electron microscopes, "SEM, JSM-7500F, Jeol, Japan", equipped with a secondary and a backscattered electron detector and "W-REM, Vega3, Tescan, Germany", equipped with a secondary electron and an EDX detector. For TEM analysis ("Spirit transmission electron microscope, FEI, USA"), samples were resuspended in distilled water containing bovine serum albumin. A 4 μL suspension was applied to glow discharged holey carbon films and blotted with filter paper. TGA analysis was carried out on a DSC-TGA 3 (Mettler Toledo, USA).

ASSOCIATED CONTENT

Ⓢ Supporting Information

The Supporting Information is available free of charge at https://pubs.acs.org/doi/10.1021/acsnano.0c01606.

> Particle count per area and particle diameters in dependence on the number of DCs, relation between laser pulse fluence and particle mass dragged from the surface into the CNT network during growth, dynamic of CNT growth for two-dimensional and three-dimensional dewetted areas (PDF)

AUTHOR INFORMATION

Corresponding Author

Norbert A. Hampp − Department of Chemistry, Philipps-University of Marburg, 35032 Marburg, Germany; Material Science Center, 35032 Marburg, Germany; ⓘ orcid.org/0000-0003-1614-2698; Phone: +49-6421-28-25775; Email: hampp@uni-marburg.de

Authors

Michael Dasbach − Department of Chemistry, Philipps-University of Marburg, 35032 Marburg, Germany

Markus Pyschik − Department of Chemistry, Philipps-University of Marburg, 35032 Marburg, Germany

Viktor Lehmann − Department of Chemistry, Philipps-University of Marburg, 35032 Marburg, Germany

Kristian Parey − Max-Planck Institute for Biophysics, 60438 Frankfurt, Germany

Daniel Rhinow − Department of Chemistry, Philipps-University of Marburg, 35032 Marburg, Germany; Max-Planck Institute for Biophysics, 60438 Frankfurt, Germany

Hendrik M. Reinhardt − Department of Chemistry, Philipps-University of Marburg, 35032 Marburg, Germany

Complete contact information is available at:
https://pubs.acs.org/10.1021/acsnano.0c01606

Notes

The authors declare no competing financial interest.

REFERENCES

(1) Yu, M. F.; Lourie, O.; Dyer, M. J.; Moloni, K.; Kelly, T. F.; Ruoff, R. S. Strength and Breaking Mechanism of Multiwalled Carbon Nanotubes under Tensile Load. Science 2000, 287, 637−640.

(2) White, C. T.; Todorov, T. N. Carbon Nanotubes as Long Ballistic Conductors. *Nature* **1998**, *393*, 240−242.

(3) Yoon, S. H.; Rungraeng, N.; Song, W.; Jun, S. Superhydrophobic and Superhydrophilic Nanocomposite Coatings for Preventing Escherichia Coli K-12 Adhesion on Food Contact Surface. *J. Food Eng.* **2014**, *131*, 135−141.

(4) Cho, H.; Lim, S.; Jin, H.-H.; Kwon, J.; Hong, S.-J.; Shin, C. Microstructures and High-Temperature Tensile Properties Of Mechanically Alloyed and Spark Plasma-Sintered 304SS-CNT Composite. *J. Compos. Mater.* **2018**, *52*, 2755−2766.

(5) Kim, J. H.; Hwang, J. Y.; Hwang, H. R.; Kim, H. S.; Lee, J. H.; Seo, J. W.; Shin, U. S.; Lee, S. H. Simple and Cost-Effective Method of Highly Conductive and Elastic Carbon Nanotube/Polydimethylsiloxane Composite for Wearable Electronics. *Sci. Rep.* **2018**, *8*, 1375.

(6) Gao, L.; Jiang, L.; Sun, J. Carbon Nanotube-Ceramic Composite. *J. Electroceram.* **2006**, *17*, 51−55.

(7) Meyyappan, M. Carbon Nanotube-Based Chemical Sensors. *Small* **2016**, *12*, 2118−2129.

(8) Sun, D.-M.; Liu, C.; Ren, W.-C.; Cheng, H.-M. A Review of Carbon Nanotube- and Graphene-Based Flexible Thin-Film Transistors. *Small* **2013**, *9*, 1188−1205.

(9) Wen, L.; Li, F.; Cheng, H.-M. Carbon Nanotubes and Graphene for Flexible Electrochemical Energy Storage: From Materials to Devices. *Adv. Mater.* **2016**, *28*, 4306−4337.

(10) Hwang, I.; Wang, W.; Hwang, S. K.; Cho, S. H.; Kim, K. L.; Jeong, B.; Huh, J.; Park, C. Multilevel Non-Volatile Data Storage Utilizing Common Current Hysteresis of Networked Single Walled Carbon Nanotubes. *Nanoscale* **2016**, *8*, 10273−10281.

(11) Wang, F.; Kozawa, D.; Miyauchi, Y.; Hiraoka, K.; Mouri, S.; Ohno, Y.; Matsuda, K. Considerably Improved Photovoltaic Performance of Carbon Nanotube-Based Solar Cells Using Metal Oxide Layers. *Nat. Commun.* **2015**, *6* (.), 6305.

(12) Kumar, S.; Rani, R.; Dilbaghi, N.; Tankeshwara, K.; Kim, K.-H. Carbon Nanotubes: A Novel Material for Multifaceted Applications in Human Healthcare. *Chem. Soc. Rev.* **2017**, *46*, 158−196.

(13) Rashad, A. A.; Noaman, R.; Mohammed, S. A.; Yousif, E. Synthesis of Carbon Nanotube: A Review. *J. Nanosci. Technol.* **2016**, *2*, 155−162.

(14) Sano, N.; Yamamoto, S.; Tamon, H. Cr as a Key Factor for Direct Synthesis of Multi-Walled Carbon Nanotubes on Industrial Alloys. *Chem. Eng. J.* **2014**, *242*, 278−284.

(15) Ding, F.; Bolton, K.; Rosén, A. Nucleation of Growth of Single-Walled Carbon Nanotubes: A Molecular Dynamics Study. *J. Phys. Chem. B* **2004**, *108*, 17369−17377.

(16) Hofmann, S.; Csanyi, G.; Ferrari, A. C.; Payne, M. C.; Robertson, J. Surface Diffusion: The Low Activation Energy Path for Nanotube Growth. *Phys. Rev. Lett.* **2005**, *95*, 36101.

(17) Yan, Y.; Miao, J.; Yang, Z.; Xiao, F.-X.; Yang, H. B.; Liu, B.; Yang, Y. Carbon Nanotube Catalysts: Recent Advances in Synthesis, Characterization and Applications. *Chem. Soc. Rev.* **2015**, *44*, 3295−3346.

(18) Roumeli, E.; Diamantopoulou, M.; Serra-Garcia, M.; Johanns, P.; Parcianello, G.; Daraio, C. Characterization of Vertically Aligned Carbon Nanotube Forests Grown on Stainless Steel Surfaces. *Nanomaterials* **2019**, *9* (14 pp.), 444.

(19) Vander Wal, R. L.; Hall, L. J. Carbon Nanotube Synthesis upon Stainless Steel Meshes. *Carbon* **2003**, *41*, 659−672.

(20) Karwa, M.; Iqbal, Z.; Mitra, S. Scaled-Up Self-Assembly of Carbon Nanotubes Inside Long Stainless Steel Tubing. *Carbon* **2006**, *44*, 1235−1242.

(21) Duanghathai, K.; Pisith, S.; Anucha, W.; Pannadda, N.; Sukanda, J. Growth of CNTs on Stainless Steel Particles. *JMST* **2009**, *23*, 123−126.

(22) Lepró, X.; Lima, M. D.; Baughman, R. H. Spinnable Carbon Nanotube Forests Grown on Thin, Flexible Metallic Substrates. *Carbon* **2010**, *48*, 3621−3627.

(23) Park, D.; Kim, Y. H.; Lee, J. K. Pretreatment of Stainless Steel Substrate Surface for The Growth of Carbon Nanotubes by PECVD. *J. Mater. Sci.* **2003**, *38*, 4933−4939.

(24) Wang, N.; Yao, B. D. Nucleation and Growth of Well-Aligned, Uniform-Sized Carbon Nanotubes by Microwave Plasma Chemical Vapor Deposition. *Appl. Phys. Lett.* **2001**, *78*, 4028−4030.

(25) Woo Lee, G.; Jurng, J.; Hwang, J. Synthesis of Carbon Nanotubes on a Catalytic Metal Substrate by Using an Ethylene Inverse Diffusion Flame. *Carbon* **2004**, *42*, 682−685.

(26) Karwa, M.; Iqbal, Z.; Mitra, S. Scaled-Up Self-Assembly of Carbon Nanotubes Inside Long Stainless Steel Tubing. *Carbon* **2006**, *44*, 1235−1242.

(27) Masarapu, C.; Wei, B. Direct Growth of Aligned Multiwalled Carbon Nanotubes on Treated Stainless Steel Substrates. *Langmuir* **2007**, *23*, 9046−9049.

(28) Pattinson, S. W.; Viswanath, B.; Zakharov, D. N.; Li, J.; Stach, E. A.; Hart, A. J. Mechanism and Enhanced Yield of Carbon Nanotube Growth on Stainless Steel by Oxygen-Induced Surface Reconstruction. *Chem. Mater.* **2015**, *27*, 932−937.

(29) Zimmer, K.; Böhme, R.; Ruthe, D.; Rudolph, T.; Rauschenbach, R. Local Growth of Vertically Aligned Carbon Nanotubes by Laser-Induced Surface Modification of Coated Silicon Substrates. *J. Phys.: Conf. Ser.* **2007**, *59*, 318−321.

(30) Zimmer, K.; Böhme, R.; Rauschenbach, B. Local Growth of Aligned Nanotubes at Surface Sites Irradiated by Pulsed Laser. *Phys. E* **2008**, *40*, 2223−2226.

(31) Reinhardt, H.; Hellmann, C.; Nürnberger, P.; Kachel, S.; Hampp, N. Free Form Growth of Carbon Nanotube Microarchitectures on Stainless Steel Controlled *via* Laser-Stimulated Catalyst Formation. *Adv. Mater. Interfaces* **2017**, *4*, 1700508.

(32) Fowlkes, J. D.; Kondic, L.; Diez, J.; Wu, Y.; Rack, P. D. Self-Assembly *versus* Assembly of Nanoparticles *via* Pulsed Laser Induced Dewetting of Patterned Metal Films. *Nano Lett.* **2011**, *11*, 2478−2485.

(33) Krishna, H.; Shirato, N.; Yadavali, S.; Sachan, R.; Strader, J.; Kalyanaraman, R. Self-Organization of Nanoscale Multilayer Liquid Metal Films: Experiment and Theory. *ACS Nano* **2011**, *5*, 470−476.

(34) Wu, Y.; Dong, N.; Fu, S.; Fowlkes, J. D.; Kondic, L.; Vincenti, M. A.; de Ceglia, D.; Rack, P. D. Directed Liquid Phase Assembly of Highly Ordered Metallic Nanoparticle Arrays. *ACS Appl. Mater. Interfaces* **2014**, *6*, 5835−5843.

(35) Fowlkes, J. D.; Roberts, N. A.; Wu, Y.; Diez, J. A.; Gonzalez, A. G.; Hartnett, C.; Mahady, K.; Afkhami, S.; Kondic, L.; Rack, P. D. Hierarchical Nanoparticle Ensembles Synthesized by Liquid Phase Directed Self−Assembly. *Nano Lett.* **2014**, *14*, 774−782.

(36) Zhuo, C.; Wang, X.; Nowak, W.; Levendis, Y. A. Oxidative Heat Treatment of 316L Stainless Steel for Effective Catalytic Growth of Carbon Nanotubes. *Appl. Surf. Sci.* **2014**, *313*, 227−236.

(37) Baddour, C. E.; Fadlallah, F.; Nasuhoglu, D.; Mitra, R.; Vandsburger, L.; Meunier, J.-L. A Simple Thermal CVD Method for Carbon Nanotube Synthesis on Stainless Steel 304 without the Addition of an External Catalyst. *Carbon* **2009**, *47*, 313−347.

(38) Masarapu, C.; Wei, B. Direct Growth of Aligned Multiwalled Carbon Nanotubes on Treated Stainless Steel Substrates. *Langmuir* **2007**, *23*, 9046−9049.

(39) Hashempour, M.; Vicenzo, A.; Zhao, F.; Bestetti, M. Direct Growth of MWCNTs on 316 Stainless Steel by Chemical Vapor Deposition: Effect of Surface Nano-Features on CNT Growth and Structure. *Carbon* **2013**, *63*, 330−347.

(40) Camilli, L.; Scarselli, M.; Gobbo, S. D.; Castrucci, P.; Nanni, F.; Gautron, E.; Lefrant, S.; De Crescenzi, M. The Synthesis and Characterization of Carbon Nanotubes Grown by Chemical Vapor Deposition Using a Stainless Steel Catalyst. *Carbon* **2011**, *49*, 3307−3315.

(41) Zhang, Q.; Zhao, M.-Q.; Huang, J.-Q.; Liu, Y.; Wang, J.; Qian, W.-Z.; Wei, F. Vertically Aligned Carbon Nanotube Arrays Grown on a Lamellar Catalyst by Fluidized Bed Catalytic Chemical Vapor Deposition. *Carbon* **2009**, *47*, 2600−2610.

(42) De Volder, M.; Park, S.; Hart, A. J. Strain-Engineered Manufacturing of Freeform Carbon Nanotube Microstructures. *Nat. Commun.* **2014**, *5*, 4512.

(43) Qu, J.; Zhao, Z.; Wang, X.; Qiu, J. Tailoring of Three-Dimensional Carbon Nanotube Architectures by Coupling Capillarity-Induced Assemble with Multiple CVD Growth. *J. Mater. Chem.* **2011**, *21*, 5967−5971.

(44) Kong, J.; Soh, H. T.; Cassell, A. M.; Quate, C. F.; Dai, H. Synthesis of Individual Single-Walled Carbon Nanotubes on Patterned Silicon Wafers. *Nature* **1998**, *395*, 878−881.

(45) Fan, S.; Chapline, M. G.; Franklin, N. R.; Tombler, T. W.; Cassel, A. M.; Dai, H. Self-Oriented Regular Arrays of Carbon Nanotubes and Their Field Emission Properties. *Science* **1999**, *283*, 512−514.

(46) Teo, K. B. K.; Chhowalla, M.; Amaratunga, G. A. J.; Milne, W. Uniform Patterned Growth of Carbon Nanotubes without Surface Carbon. *Appl. Phys. Lett.* **2001**, *79*, 1534−1536.

(47) Hofmann, S.; Cantoro, M.; Kaempgen, M.; Kang, D.-J.; Golovko, V. B.; Li, H. W.; Yang, Z.; Geng, J.; Huck, W. T. S.; Johnson, B. F. G.; Roth, S.; Robertson, J. Catalyst Patterning Methods for Surface-Bound Chemical Vapor Deposition of Carbon Nanotubes. *Appl. Phys. A: Mater. Sci. Process.* **2005**, *81*, 1559−1567.

(48) Englander, O.; Christensen, D.; Lin, L. Local Synthesis of Silicon Nanowires and Carbon Nanotubes on Microbridges. *Appl. Phys. Lett.* **2003**, *82*, 4797−4799.

(49) Rohmund, F.; Morjan, R. E.; Ledoux, G.; Huisken, F.; Alexandrescu, R. Carbon Nanotube Films Grown by Laser-Assisted Chemical Vapor Deposition. *J. Vac. Sci. Technol., B: Microelectron. Process. Phenom.* **2002**, *20*, 802−811.